Intra-Annual Variability of CH_4

Shanice Bailey & Ivan Mitevski

December 2019

Abstract

Greater climate concerns in regards of greenhouse gas emissions have been emphasized on the rapid increase of methane. Its unusual trend has been observed, particularly regarding the plateauing (during 1999-2007) in between its ever-increasing climb from 1983 to present. The source of this enigmatic plateau feature and different growth rates of methane concentrations continue to elude us due to the large uncertainties in the methane budget (Saunois et al, 2016). Methane has a seasonal cycle even during the different growth rate periods and enigmatic plateau where there is a maximum and minimum around July and November, respectively (Fig.1). This seasonal cycle is present from the time we have observations (1983) and has not received as much attention in the literature as the overall rising methane trend. The goal of this project is to investigate which sources and sinks are driving methane's seasonal cycle and to determine if emissions due to wetlands, do indeed, play a dominant role in the intra-annual variability of methane.

For this project we altered and employed the one-box model from Lab 1 and two-box model from Lab 2. The model was enabled to read in emissions and sinks using the same `RK45 solver`, and new parameter k and budget term B were added. We used wetland emissions data from WetCHARTs version 1.0, anthropogenic emissions gathered from Community Emissions Data System (CEDS) for Historical Emissions, and OH data from GFDL provided by Jian He. We forced the two models with three different conditions: 1) forcing by wetland emissions only, 2) forcing by anthropogenic emissions only, and 3) forcing by wetland and anthropogenic sources (total emissions). We also explored the dynamic relationship between the hydroxyl radical, OH, and the observed sources by changing OH concentration seasonally.

We quickly discovered the error in our assumption of wetlands acting as the main driver for CH_4 seasonality simply due to the fact that the peaks and troughs in its trend were inverse of methane's observed trend. However, we have found through our one-box run with LCH4, a strong seasonal cycle from wetland and total emissions (anthropogenic + wetlands). The two-box model run with LCH4 does not produce any strong seasonal cycles from either sources, nor from the combination of the two sources. However, our two-box runs seem to be unreliable since we needed to tune k by excessive values. Though we cannot confirm our idea that wetland emissions drive CH_4 seasonality, we postulate that it can serve as a proxy for CH_4 trending, by reasoning that the system driving wetland emission variability is the same system driving methane seasonality.

1 Introduction

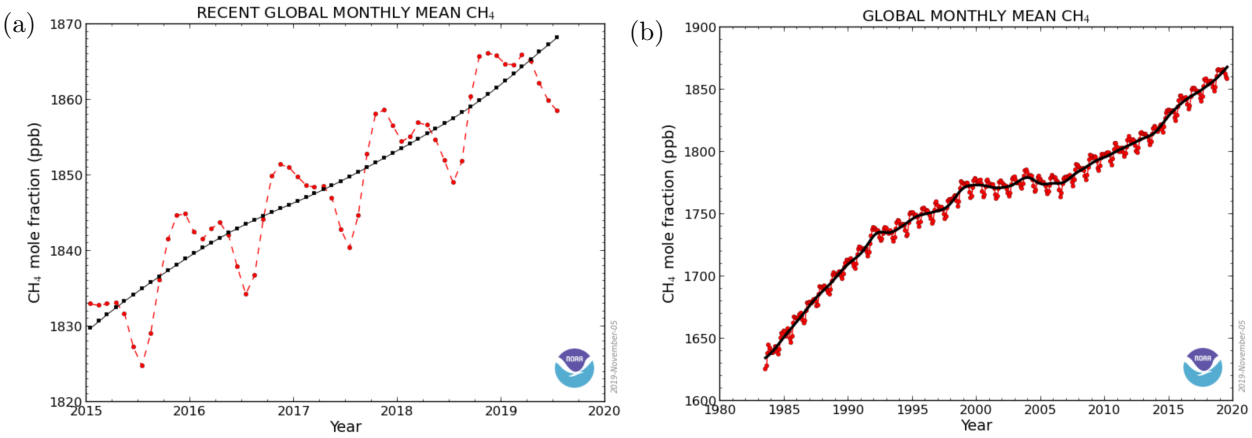

Figure 1: Monthly CH_4 observations from NOAA ESRL for **a)** 2015 to 2019 and **b)** 1983 to 2019.

Methane is a major anthropogenic greenhouse gas and plays a key role in the production of tropospheric ozone (Foster et al., 2007) - its contribution to anthropogenic climate forcings is about half of CO_2 (Prather et al. 2017). The main sources of CH_4 are wetlands, agriculture, industry production, energy derived from fossil fuels, transportation, commercial, waste and international shipping (Denman et al., 2007). Methane concentrations have increased from 720 ppb in pre-industrial era (Prather et al. 2017) to 1865 ppb in 2019 (Fig. 1b). Atmospheric methane shows a rise from 1983 to 1999, then plateaus until 2007, only to return to a rising trend up to present, (Fig. 1b). Due to the large uncertainties in the methane budget it remains unclear why we observe the different growth rates and plateau feature in CH_4 trend (Saunois et al., 2016). The sources for these uncertainties are: wetlands; partitioning among regions; decadal changes in both natural and anthropogenic emissions; and chemistry models used to infer emissions from observations.

From Fig. 1a and Fig. 2 we can see that methane has a persistent seasonal cycle that peaks around November/December and has a minimum around July/August even during the different growth rate periods and plateau. This seasonal cycle is present since the time we have observations (1983) and has not received as much attention as the overall rising methane trend. Adhering to recent literature of the importance of methane emissions from both natural and anthropogenic wetland sources (Bousquet et al., 2006; Nisbet et al., 2016; and Poulter et al., 2017), we believe it is this source that drives the intra-annual variability of CH_4 concentrations.

Wetlands are the largest natural source of global methane emissions (Poulter et al., 2017). From isotopic evidence presented in Nisbet et al., 2016, it has been proposed that the likely cause for the observed increase after the 8-year plateau was due to the expansion of wetland extent during years of anomalously strong rainfall. Bousquet et al., 2016, found that fluctuations in methane emissions drove the interannual variability in surface CH_4 emissions. Following these notions of wetlands' global influence on the interannual timescale, we expected to find further investigation of the wetlands' effect on the intra-annual variability in surface CH_4 emissions. Such literature is insubstantial and lacking.

For the scope of this class project, and through the use of valuable simple box models, the goal of this project is to investigate which sources and sinks are driving methane's seasonal cycle and to determine if emissions due to wetlands, do indeed, play a dominant role in the intra-annual variability of methane. Though we did not use complex, coupled, atmospheric chemistry models, we believe the simple box models, nevertheless, provide insight to the inherent influence of different methane emission sources.

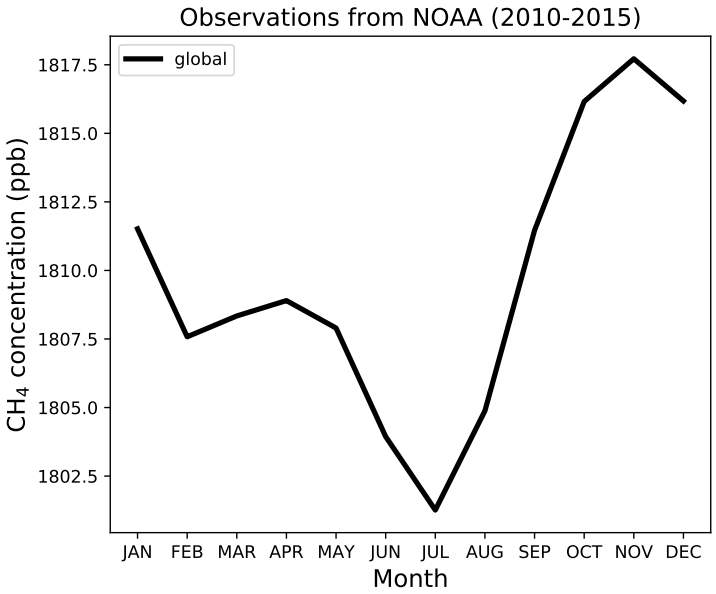

Figure 2: CH_4 monthly concentration averaged over 2010-2015 from NOAA. Methane reaches a local minimum during July and achieves a peak around November.

2 Methods

2.1 One-box Model

We endeavored for the first stage of this project to reproduce the seasonal trend we observe from NOAA's data (Fig. 2), by adopting the simplified, one-box model of CH_4 concentration from Lab 1. The rate of change of CH_4 concentration, in its simplest form, can be derived from the conservation of mass continuity equation, elucidating that the source emissions into the system is countered by the sinks removing methane from the system. Our one-box model, therefore, can be expressed as

$$\frac{dM}{dt} = E - k_*[OH]M, \tag{1}$$

where M is the mass of CH_4 in the system, measured in Tg; E are the source emissions in Tg/month, [OH] is the concentration of the hydroxyl radical, OH (ppb), k_* (1/time) represents the rate constant for OH+CH_4 reaction, and the last term represents the total loss in CH_4 concentrations.

We explored how the system reacted with different sources in three separate conditions by modifying the one-box model to run with observation data. We forced the model to run with only wetland emissions (data from WetCHARTs version 1.0); only anthropogenic emissions (data gathered from Community Emissions Data System (CEDS) for Historical Emissions); and the summation of both.

We also explored the dynamic relationship between the hydroxyl radical, OH, and the observed sources by changing OH concentration seasonally (data provided by Jian He). The OH dataset is averaged monthly over the 2012-2017 time period. Both wetland and anthropogenic data are averaged monthly over the 2010-2014 time period.

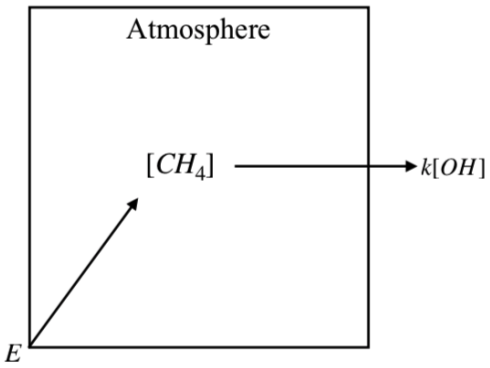

Figure 3: Diagram of the 1-box model. E represents the emissions into the atmosphere box and $k[OH]$ represents the chemical loss rate.

2.2 Two-box Model

Taking a step closer to real-world conditions, we consider a system of two hemispheres. The two-box model adopted from Lab 2 allow us to survey the latitudinal distribution of each emission source, and determine the relative influence of either hemisphere. Evoking the continuity equation and expanding its application for two interdependent systems, equation 1 becomes

$$\frac{dM_{NH}}{dt} = E_{NH} - k[OH]_{NH}M_{NH} + \frac{M_{SH} - M_{NH}}{\tau} \tag{2}$$

$$\frac{dM_{SH}}{dt} = E_{SH} - k[OH]_{SH}M_{SH} + \frac{M_{NH} - M_{SH}}{\tau}, \tag{3}$$

where NH and SH denotes Northern and Southern hemisphere, respectively, the last terms in equation 2 and 3 represent the inter-hemispheric exchange rate, and the rest of the parameters represent the same variable from equation 1 for their respective hemispheres. We applied similar procedures from the one-box model for the two-box model runs.

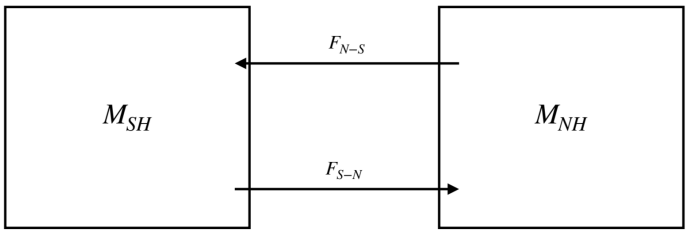

Figure 4: Diagram of two-box model. M_{NH} and M_{SH} represents the mass of CH_4 concentration in NH and SH box, respectively. F_{N-S} and F_{S-N} represent the inter-hemispheric exchange (last terms in equation 2 and 3).

2.3 One-box model run with LCH4

This one-box model run represents the total loss of CH_4 (now dependent on temperature):

$$\frac{dM}{dt} = (E - B) - k[\text{LCH4}] \tag{4}$$

where M is the mass concentration, E are the emissions (total, anthropogenic only, and wetlands only), k is the tuning parameter used to adjust the budget, and B is the budget term which is the difference between

the mean emissions and mean losses over the 5-year period 2010-2014. We tried to set the budget to make emissions and losses achieve as close to a balanced system as possible, so that we can run the model for more than 1 year. The tuning parameter k is used to try and achieve desired steady state at the end of the 5-year run. We will note, the budget term, B, is not enough to set the budget in some cases because it represents the mean over 5 years and the model is run for 60 months.

2.4 Two-box model run with LCH4

Next, we expanded our system to represent two hemispheres via our two-box model. We simulate the same three conditions as was done with the one-box model; and we also consider LCH4 in our system. The governing equations for our two-box system are as follows:

$$\frac{dM_{nh}}{dt} = (E_{nh} - B_{nh}) - k\text{LCH4}_{nh} + \frac{M_{sh} - M_{nh}}{\tau}$$
$$\frac{dM_{sh}}{dt} = (E_{sh} - B_{sh}) - k\text{LCH4}_{sh} + \frac{M_{nh} - M_{sh}}{\tau}$$

where M is the mass concentration, E are the emissions (total, anthropogenic only, and wetlands only), k is the tuning parameter used to adjust the budget, B is the budget term which is the difference between the mean emissions and mean losses over the 5-year period, 2010-2014, and τ is the inter-hemispheric exchange rate. The tuning parameter, k, is adjusted to achieve the same goal as was desired in the one-box model - to balance the sources with the sinks.

3 Results and Discussion

Very early on we found that our initial hypothesis of wetland sources being the primary driver of CH_4 concentrations was flawed. Fig. 5a proves contrary to our original thought because we see global CH_4 concentrations (black link) peaking during the summer months (July/August) which coincides with the observed global methane trend reaching a local minimum. Subsequently, we observed that WetCHARTs v1.0 wetland emissions reaches a minimum around the same time (November through January) NOAA's global methane emissions peak at its maximum.

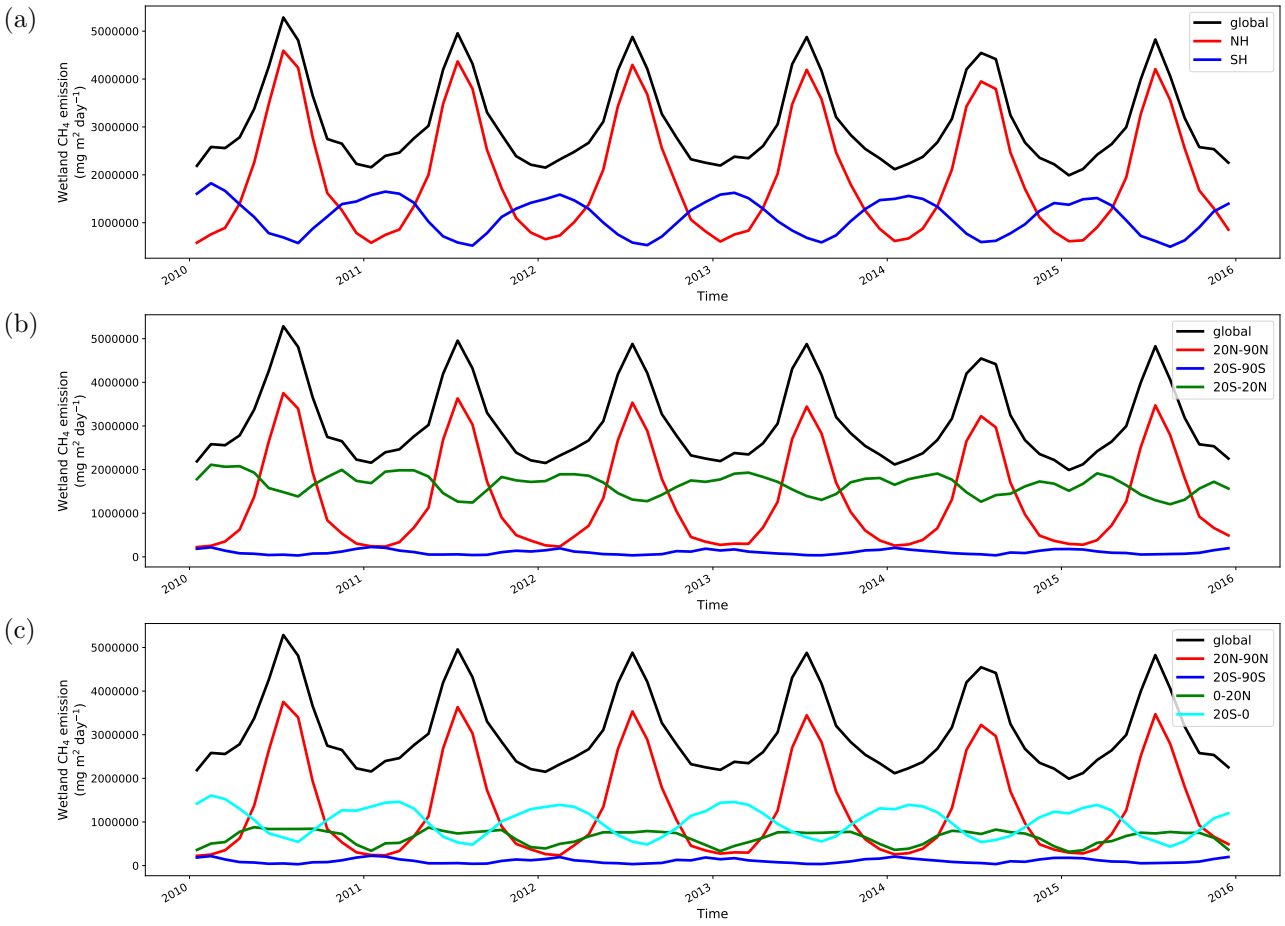

Figure 5: Wetland emissions (mg m^2 day^{-1}) for **a)** global, NH, and SH; **b)** 20-90 latitude in both hemispheres and tropics (20S-20N); and **c)** for 0-20N and 0-20S latitude.

Naturally, this came as a surprise. We then became curious about how wetland emissions behaved in each hemisphere. The Northern hemisphere (red line) in Fig. 5a seems to have the dominant impact on global methane concentrations since its trend most resembles the global trend. As expected simply due to the hemispheres experiencing opposite seasons, the Southern hemisphere's trend (blue line) was an antipode to the Northern hemisphere, though not equal in magnitude. Concentrations in the Northern hemisphere peaked around $4.5e10^6 \frac{mg}{m^2\ day}$; whereas, the peaks in the southern hemispheres occurred around $1.5e10^6 \frac{mg}{m^2\ day}$.

We further broke down the hemispheres to consider the roles of the tropics, defined as a band between 20°S and 20°N. We instantly noticed that the concentrations in the Southern hemisphere decreased to peaking around the same level concentrations in the Northern hemisphere reach its minimum at $3e10^5 \frac{mg}{m^2\ day}$. To further determine the extent of dominance of Northern hemispheric concentrations on global emissions, we divided the tropical band to a northern and southern tropical band. Unexpectedly, it is the southern tropical band that has first order influence on tropical emissions; however, upon further thought, it is the 20°S-0° band that emits more CH_4 than the 0°-20°N band because of the severe anthropogenic activity (i.e. forest clearing and livestock activity).

From the CEDs and WetCHARTs v1.0 data, we considered both anthropogenic and wetland sources since we deduced from the literature that these are the two strongest areas for global CH_4 emissions. Fig. 6 shows the seasonality of their respective global and hemispheric CH_4 concentrations (Fig. 6a and 6b), as well as the seasonality of CH_4 concentrations from the combination of the two sources (Fig 6c), and OH seasonality (Fig 6d).

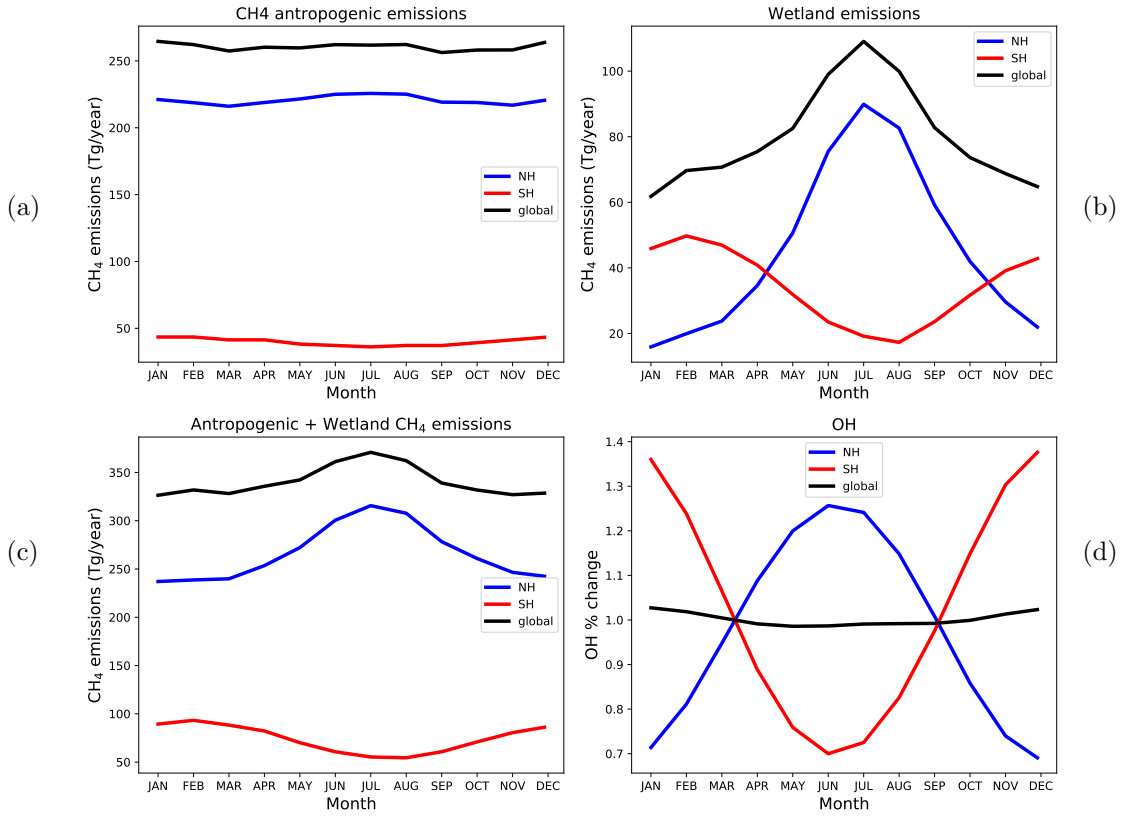

Figure 6: Monthly CH_4 emissions (Tg/year) from **a)** anthropogenic, **b)** wetland sources, and **c)** both anthropogenic and wetland sources all averaged over 2010-2015. **c)** Monthly OH ratio (to respective mean) global, NH and SH averaged over 2012-2017 from GFDL model.

We can see that averaged anthropogenic sources express very little seasonality; while, as previously stated, wetland emissions show opposing seasonality to NOAA's observed CH_4 emissions. The combination of anthropogenic and wetland sources in Fig. 6c shows a dampened seasonality from Fig. 6b. In Fig. 6c, OH global seasonality is similar to global anthropogenic emissions in regards to expressing a relatively unchanging trend throughout the year. This is due to the concentrations in the two hemispheres cancelling each other out: Northern hemispheric concentration peaks during summer months with a maximum of 1.25 of the mean while Southern hemisphere concentrations reach minimum of around 0.7 of the mean value.

3.1 One-box Model

We considered three conditions under which to run our one-box model: forcing the run with 1) only wetland emissions; 2) only anthropogenic emissions; and 3) a combination of the two sources. Using the one-box model to reproduce the seasonality observed from NOAA's global CH_4 emissions, we find from Fig 7.b that the runs with only wetland data and only anthropogenic data did not show any seasonality. However, when we consider both sources and a chosen optimal reaction rate constant, $k = 0.073$, we can see that the third run has a similar seasonal pattern to the observations (Fig. 7.a). The third run (black line) peaks over 1820ppb around October-November, and reaches a minimum below 1790ppb during May. Observations (purple, dashed line) peak a little later around November-December at 1817ppb and reach a minimum near 1800pbb during July. It has to be noted that this run was tuned by choosing the appropriate parameter $k = 0.073$ so the shape of the curve can match the observations. In case we allow k to vary as a function of concentration, we can fit observations with relatively very small error.

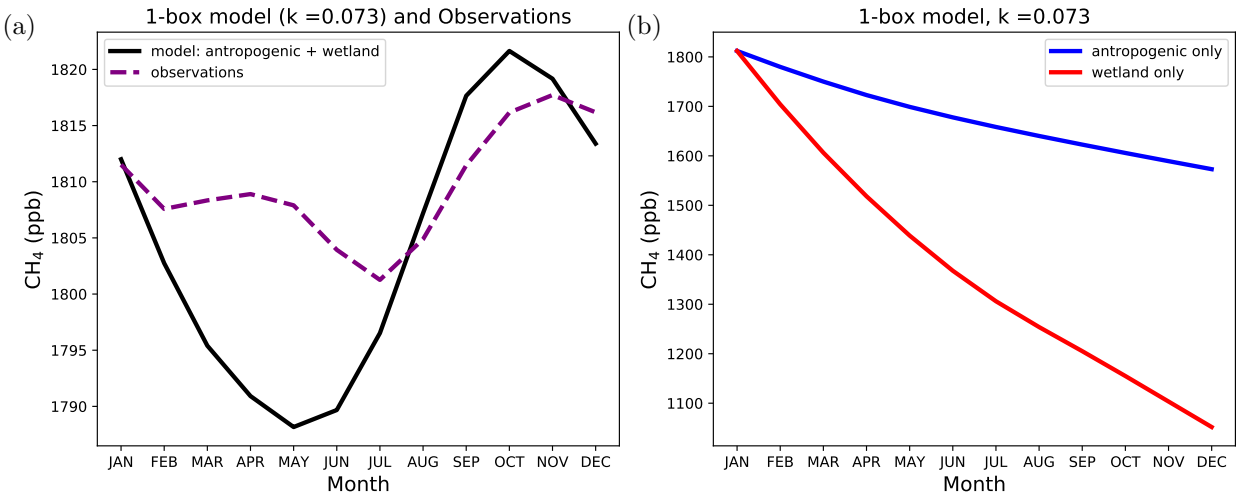

Figure 7: **a)** 1-box model run for 12 months using equation (1) with $k = 0.073$ where emissions E are the sum of anthropogenic and wetland sources (purple dashed line) compared with monthly observations (black line) averaged from 2010-2015. **b)** Same model run with only anthropogenic and wetland emissions shown with blue and red lines, respectively.

Figure 8 shows model runs with antropogenic only and wetland emissions only where they are compared to observations. Parameer k was carefully chosen here to match observations as much as possible. For the anthropogenic and then wetlands run, it was determined k=0.056 and k=0.017, respectively, to be matching observations best.

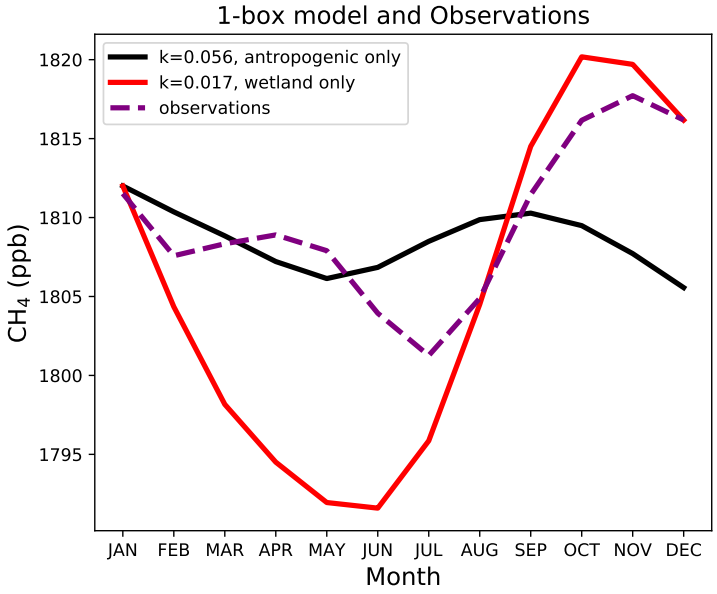

Figure 8: 1-box model run for anthropogenic only (black line) for $k = 0.056$, wetlands only (red line) for $k = 0.017$ compared to observations (dashed purple)

3.2 Two-box Model

Fig. 9 shows the third-condition run (model forced with both anthropogenic and wetland emissions) using the two-box model. We can see that the two hemispheres are equal and opposite. The Northern

hemisphere achieves largest CH_4 concentrations of 1901.4ppb during April, while the Southern hemisphere achieves lowest CH_4 values of 1899.1ppb during April and September. This run seems highly unlikely to emulate reality; however, it was best we could do with tuning k to be conserving the budget of sources and sinks.

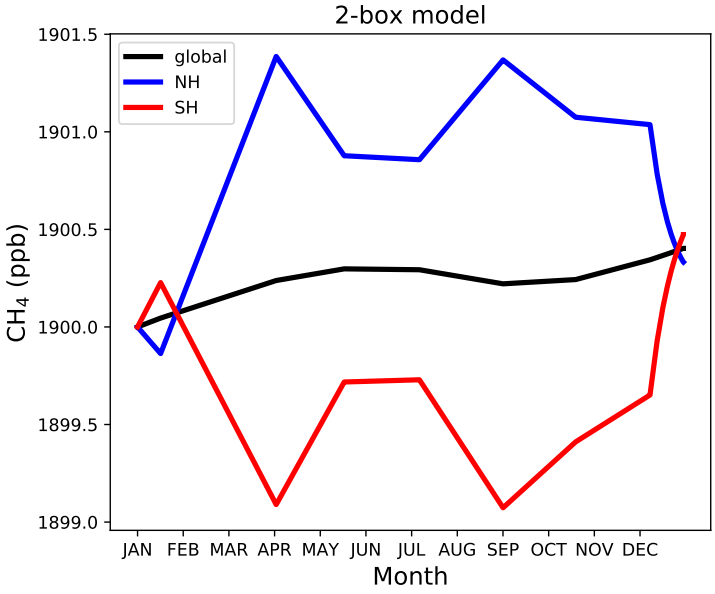

Figure 9: Two-box model run of CH_4 emissions in NH, SH, and global over 12 months in blue, red, and black lines respectively.

3.3 One-box model run with LCH4

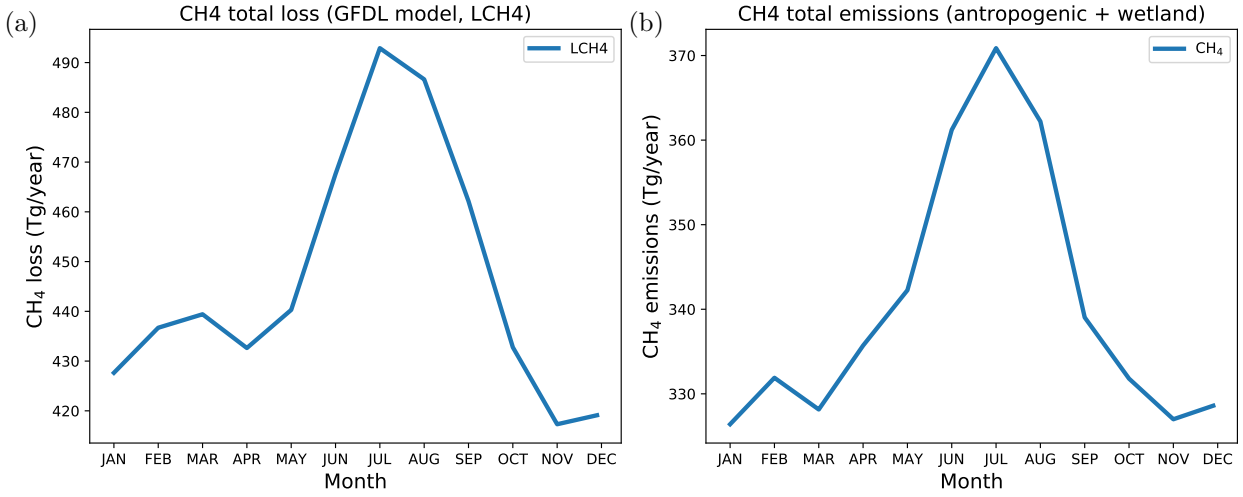

Figure 10: **a)** CH_4 total loss (LCH4) taken from GFDL model as monthly average over 2012-2017. **b)** CH_4 total emissions (antropogenic and wetlands) as monthly average over 2010-2014

Fig.10.a shows that CH_4 total loss peaks during July/August months and the total emissions in Fig. 10b also peak during July. The total emissions seem to be more equally distributed at the beginning (Jan-Mar) and the end of the year (Oct-Dec), rather than the total loss where LCH4 reaches a minimum at the end of

the year around November time. The imbalance of sinks and losses (more sources than sinks) at the end of the year may be driving the seasonal peak and the end of the year (Fig.1).

3.3.1 Total emissions (anthropogenic + wetland)

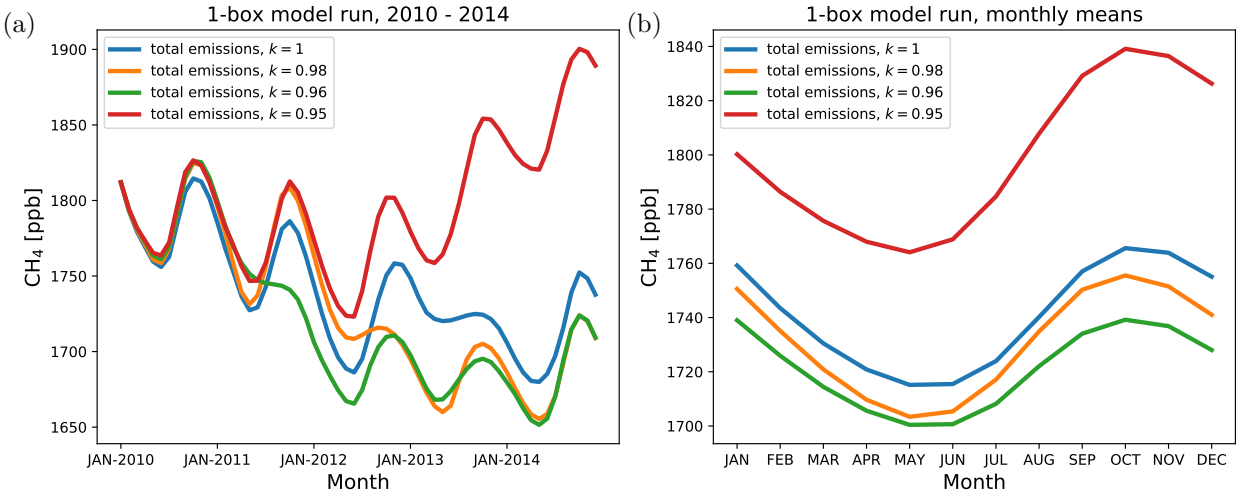

Figure 11: **a)** 5-year timeseries of one-box model run from 2010-2014. **b)** Monthly averages of the one-box model run from 2010-2014. The two types of runs are computed with $k = 1, 0.98, 0.96, 0.95$

.

Fig. 11 illustrates the influence of the tuning parameter, k. Increasing k means the strength of the sink term from equation 4 increases; and vice versa, a decrease in k diminishes the sink's strength, which leads to the "bounce-back" of CH_4 emissions (Fig. 11.a, k=0.95). When k=1 we see that our budget is not in balance, and this is because the model runs for 60 months, however, the budget that we calculated at each time step is taken as the mean over a 5-year time interval.

We also notice that the total emissions show a strong seasonal cycle which is consistent for the range of values for k used (1, 0.98, 0.96, 0.95). Even when the total emissions and sinks are not well balanced ($k = 0.95$) there still persists a seasonal cycle (red lines in both panels in Fig.11). We continue on to run the model under the last two conditions (with only anthropogenic and only wetland emissions) to determine if the seasonal cycle persists with the individual sources. We acknowledge the limitations of running the model separately with different emission sources because the overall sinks are held constant (for each month). In order to maintain a balance between the emission and sources we are using the free parameter k, to weaken or strengthen the sink as needed.

3.3.2 Anthropogenic Emissions only

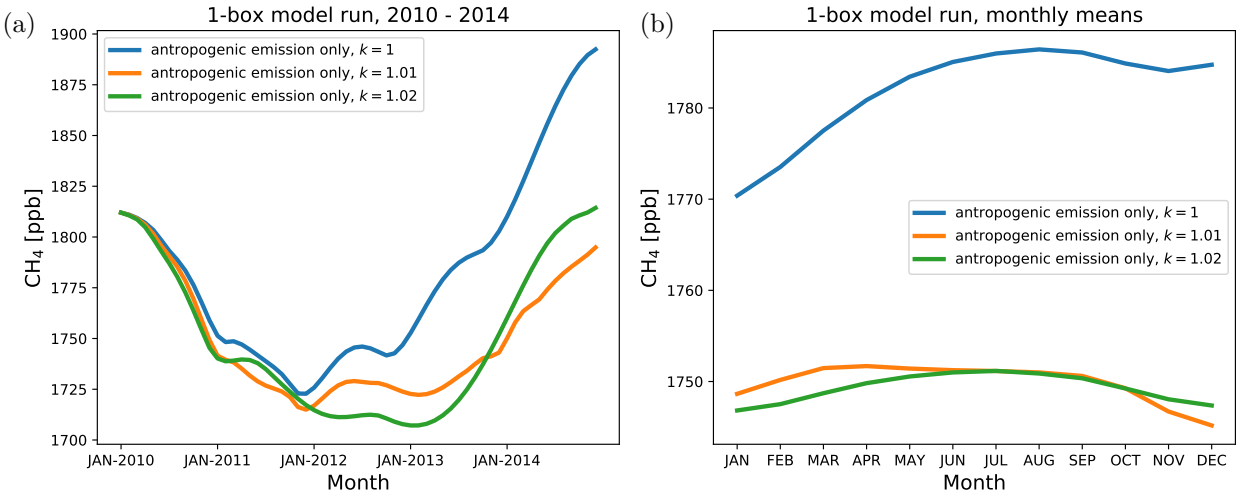

Figure 12: **a)** Timeseries of 1-box model run with **anthropogenic emissions only** from 2010 - 2014. **b)** Monthly means of 1-box model run from 2010 - 2014 with **anthropogenic emissions only**. In both cases runs are with $k = 1, 1.01, 1.02$

In the model run with only anthropogenic emissions we observe no seasonality (Fig.12.b). The 5-year timeseries shows an overall minimum around mid-2012 (Fig. 12a), and the monthly averages (Fig.12b) show maximum near mid-year for $k = 1.01$ and $k = 1.02$. The run for k=1 shows that we need to increase the sink (we have less sources in this case) and therefore, we need to relax the sink in order to achieve a balance between the two endpoints (2010 and end of 2014). This is achieved when $k > 1$, specifically, when k=1.02.

3.3.3 Wetland Emissions only

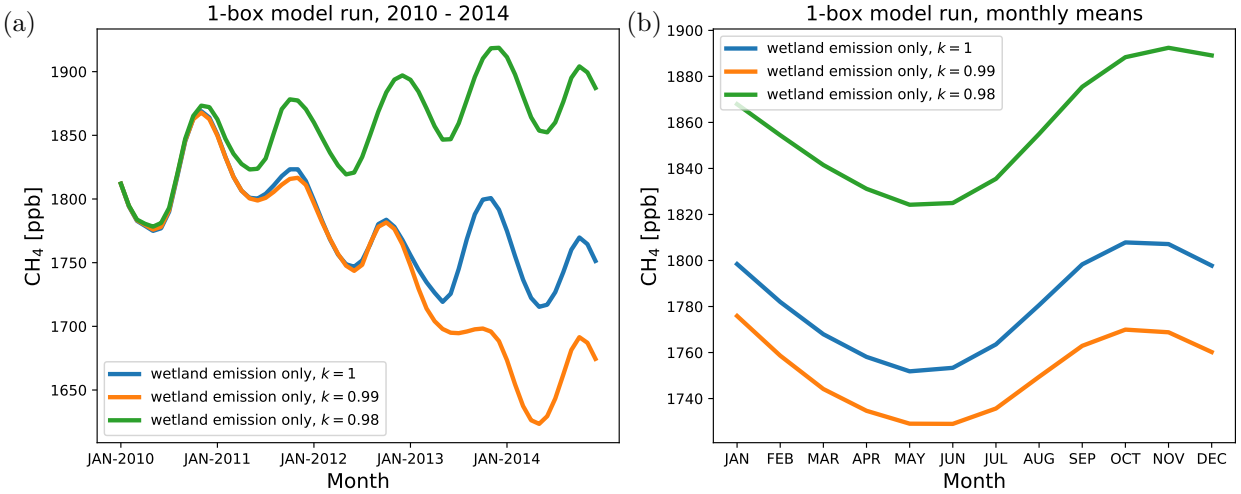

Figure 13: **a)** Timeseries of 1-box model run with **wetland emissions only** from 2010 - 2014. **b)** Monthly means of 1-box model run from 2010 - 2014 with **wetland emissions only**. In both cases runs are with $k = 1, 0.99, 0.98$

The model run with only wetland emissions produces a strong seasonal cycle which has a minimum around mid-year (June), similar to that of the minimum reached during July from the observations.

3.4 Two-box model run with LCH4

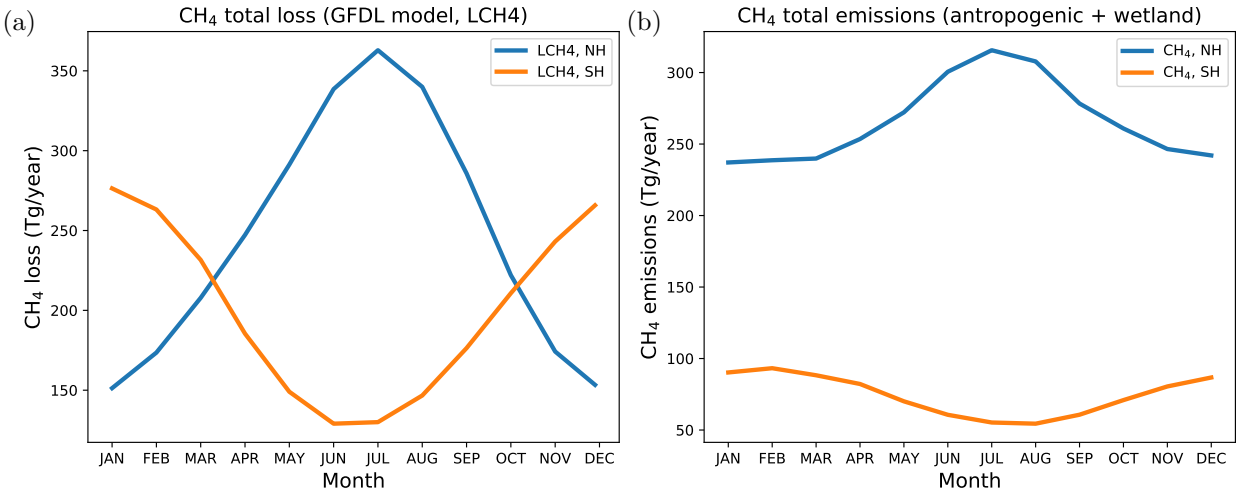

Figure 14: **a)** CH_4 total loss (LCH4) for NH and SH taken from GFDL model as monthly average over 2012-2017. **b)** CH_4 total emissions (anthropogenic and wetlands) for NH and SH taken as monthly average over 2010-2014

For the two-box model we expand our system into two hemispheres (NH and SH). We can see from Fig.14a the two hemispheres are dichotomous as is to be expected. Similar to the one-box model run of total CH_4 loss, in Fig. 10a we see the NH peak during summer months June-August, and the SH peaks during boreal winter (November-February). Shifting our focus over to Fig. 14b, we can see there is little seasonality compared to what we've seen in the one-box run for total CH_4 emissions (Fig. 10b).

3.4.1 Total emissions (anthropogenic + wetland)

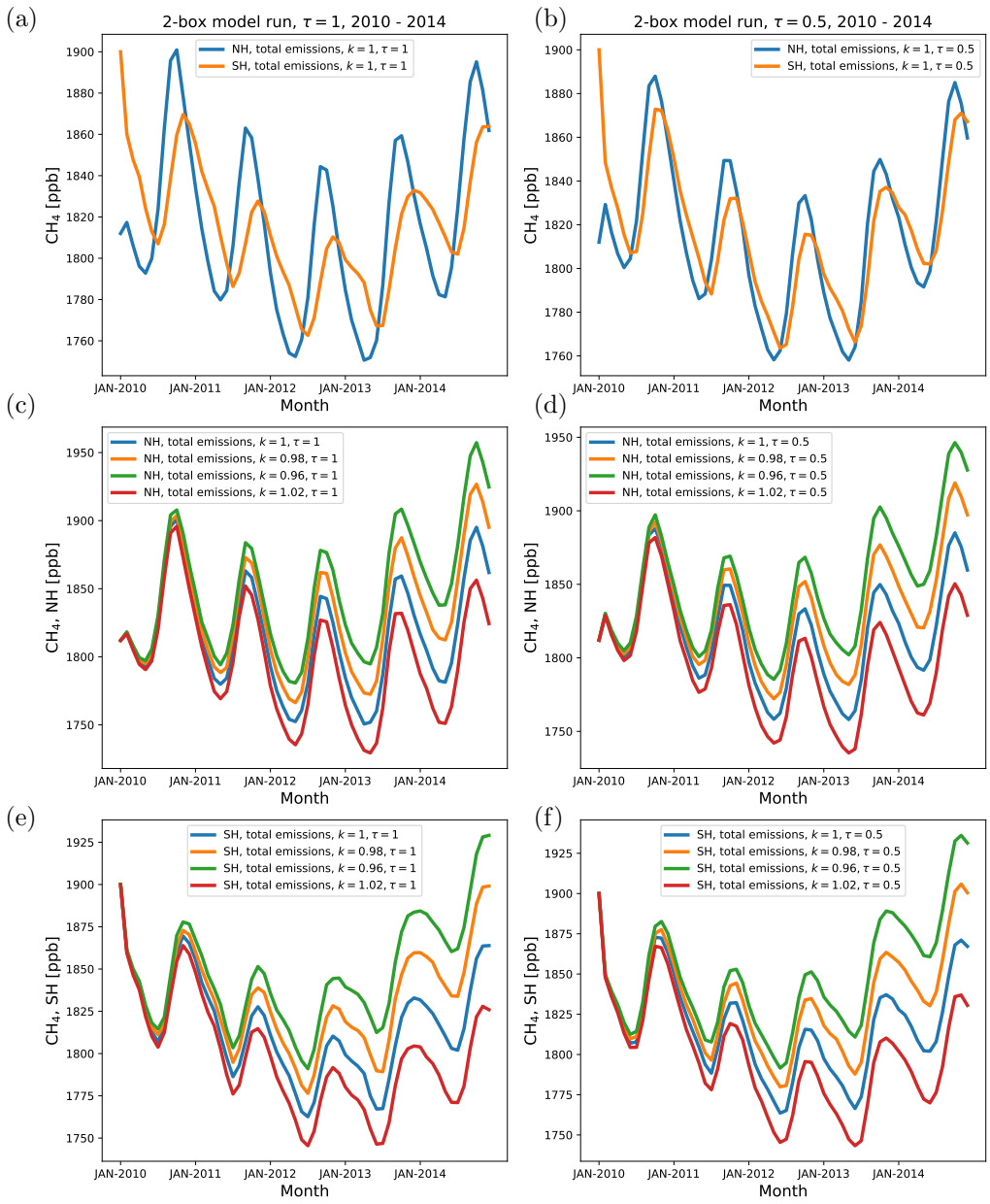

Figure 15: Two-box model run of hemispheric total emissions for 5 years (2010 - 2014) using LCH4 for NH and SH where k and τ are varied. Left and right column show $\tau = 1$ and $\tau = 0.5$, respectively. First row shows the timeseries for both hemispheres, second row shows the timeseries for NH, and third row shows the timeseries for SH.

Fig. 15 shows the results from the two-box model run for the 5-year interval of total emissions (anthropogenic + weltand) with values of k=1, 0.98, 0.96, 1.02 and the interhemispheric exchange rate, τ=0.5, 1. Lower values of τ means the inter-hemispheric transport increases, that is why we observe total emissions in both hemispheres to be closer to value when τ=0.5 (Fig. 15b), than when τ=1 (Fig. 15a). We observe strong seasonality in all the panels. Results seem robust for different values of τ and k.

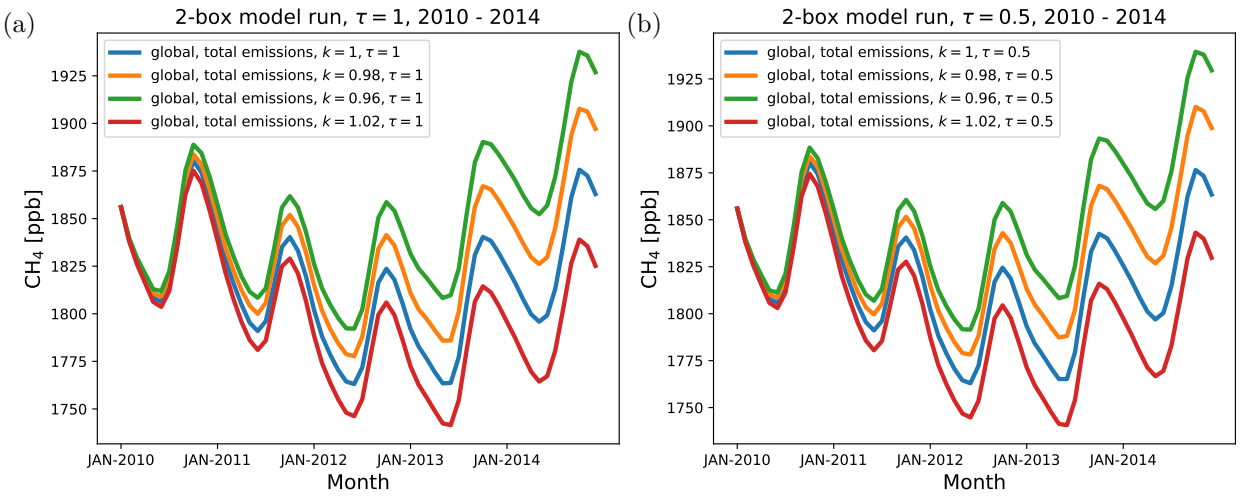

Figure 16: Two-box model run of global total emissions for 5 years (2010 - 2014) using LCH4 for global values where k and τ are varied.

Fig. 16 shows the timeseries of the global CH_4 emissions (NH+SH) for τ=0.5 and 1. We can see that emissions peak towards the end of the year and reach a minimum during the summer months - this is similar to what we observe in the NOAA observations (Fig. 2). An interesting observation we would like to point out is the strange slope in the third row of Fig. 15 during mid-2012 to mid-2013. This pattern is reminiscent to what we see in Fig 1.a during 2017. We don't observe this pattern in the NH panels, nor in Fig. 16.

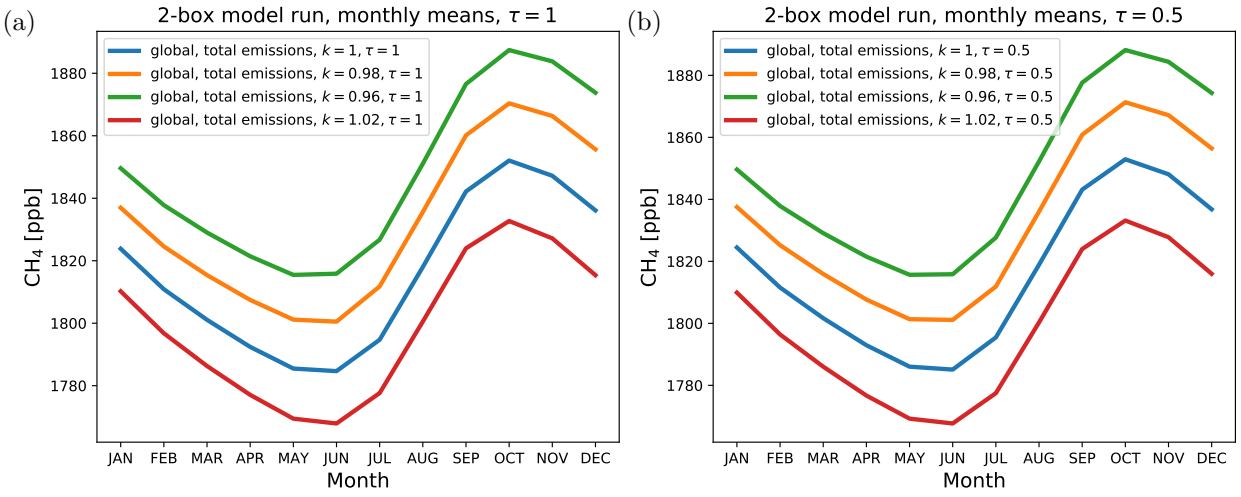

Figure 17: Monthly means of two-box model run of global total emissions for 5 years (2010 - 2014) using LCH4 for global values where k and τ are varied.

In Fig. 17, we've shown monthly averages of the global emissions, and observe a minimum during May-June and a maximum during October-November months. This seasonal trend is very similar to the observed, and to the trend produced from the one-box model run using LCH4. Next, we ran the two-box model with only anthropogenic emissions; then only wetlands emissions.

3.4.2 Anthropogenic Emissions only

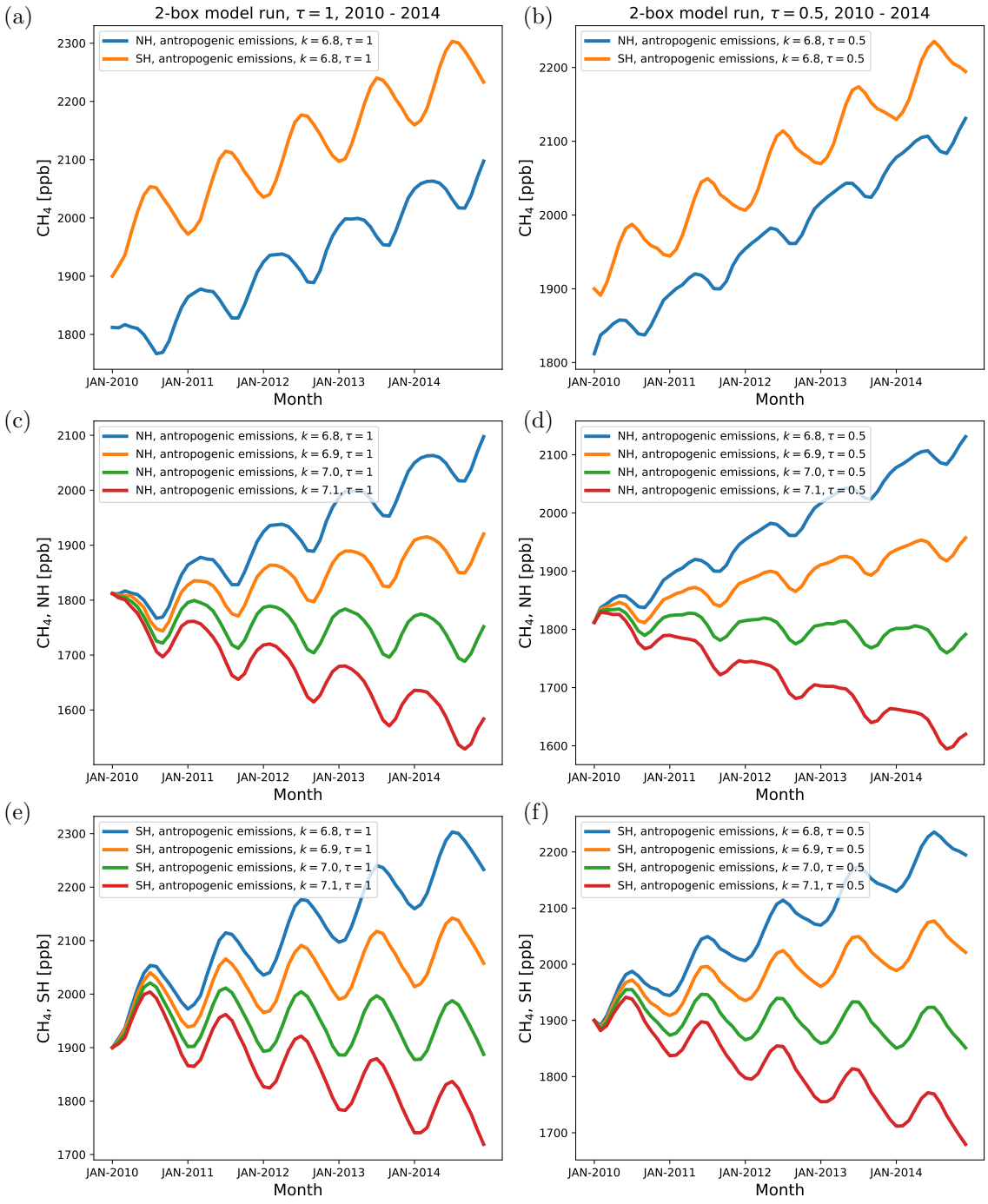

Figure 18: Two-box model run of hemispheric anthropogenic emissions for 5 years (2010 - 2014) using LCH4 for NH and SH where k and τ are varied. Left and right column show $\tau = 1$ and $\tau = 0.5$, respectively. First row shows timeseries of both hemispheres, second row shows the timeseries for NH, and third row shows the timeseries for SH.

We observe interannual variability in both hemispheres for the anthropogenic run (Fig. 18). Oddly, the SH emulates the observed seasonal trend and the NH follows the opposite trend. This observation is

unsettling because we have shown that the NH is the dominant hemisphere (Fig. 5).

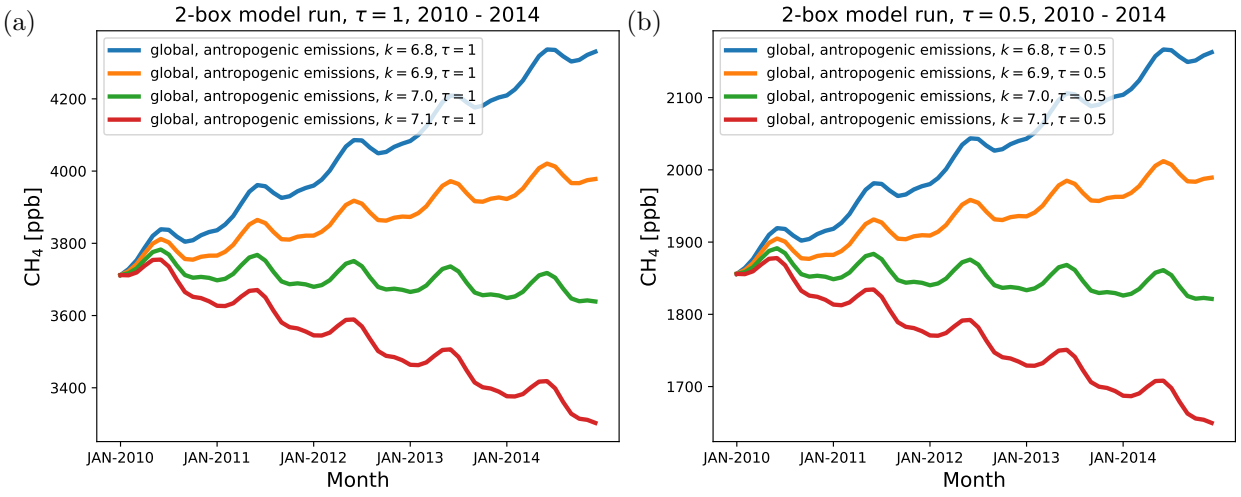

Figure 19: Two-box model run of global anthropogenic emissions for 5 years (2010 - 2014) using LCH4 for global values where k and τ are varied.

We can see a consistent interannual trend from the global anthropogenic emissions (Fig. 19). The peaks occur during the spring time of the years and reach a minimum during late-summer, winter months. This is unlike the trend seen in observations (Fig. 2). In Fig. 20, we have shown monthly averages of the global anthropogenic emissions, and observe little to no seasonality, with a minimum occurring during the months of November-December and a maximum achieved during May-June months. This trend is quite different from the seasonality observed from considering total emissions (anthropogenic + wetlands) and the observed (Fig. 17 and Fig. 2).

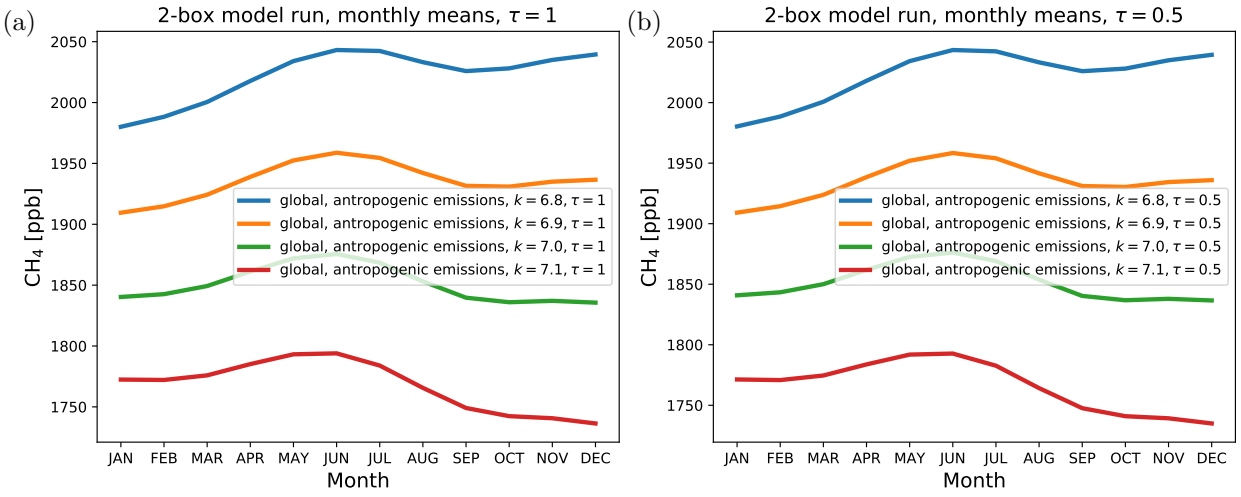

Figure 20: Monthly means of two-box model run of global anthropogenic emissions for 5 years (2010 - 2014) using LCH4 for global values where k and τ are varied.

3.4.3 Wetland Emissions only

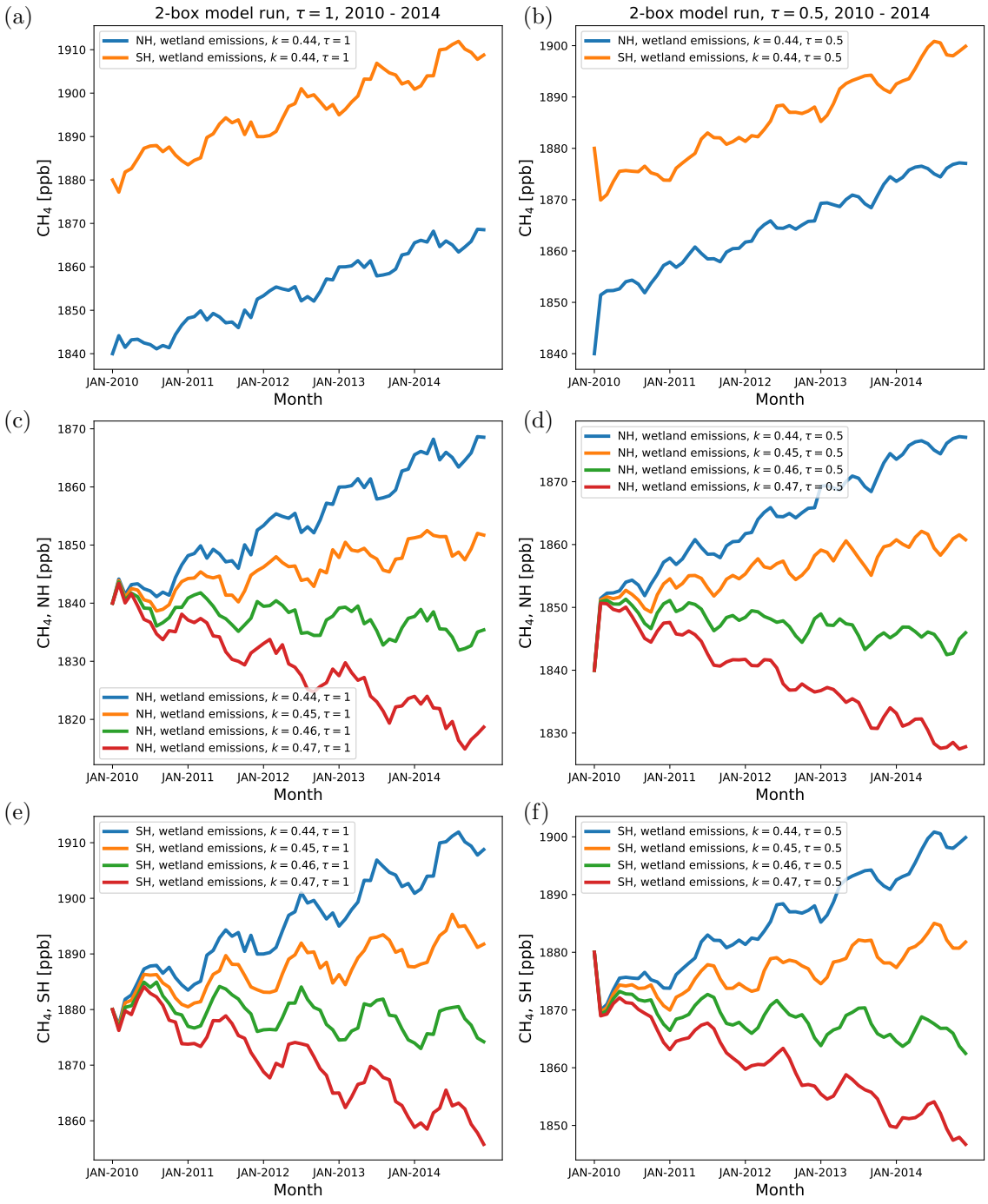

Figure 21: Two-box model run of hemispheric wetland emissions for 5 years (2010 - 2014) using LCH4 for NH and SH where k and τ are varied. Left and right column show $\tau = 1$ and $\tau = 0.5$, respectively. First row shows timeseries of both hemispheres, second row shows the timeseries for NH, and third row shows the timeseries for SH.

Focusing on wetland emissions only, our two-box run produced a more intra-variable trend than for either anthropogenic emissions only run and total emissions run. We notice, the general wetland emissions trend

(peaks and troughs) are inverse to that of the total emissions run (Fig. 15), with its peaks occurring during the middle, and troughs during the beginning of each year.

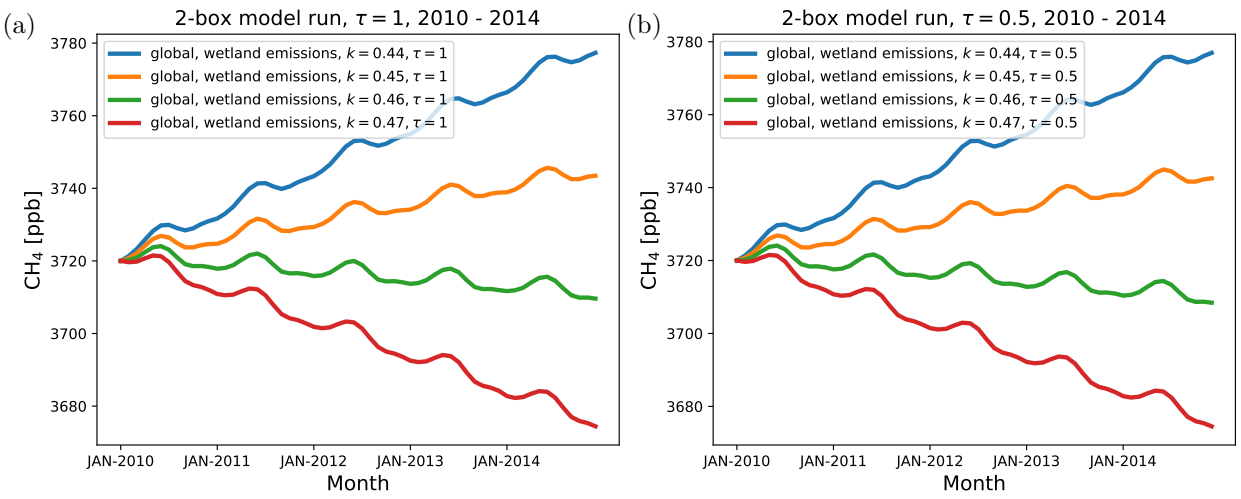

Figure 22: Two-box model run of global wetland emissions for 5 years (2010 - 2014) using LCH4 for global values where k and τ are varied.

The global wetland emissions trend (Fig. 22) is similar to that seen from global anthropogenic emissions (Fig. 19). Likewise, this trend looks unlike the observations. Another similarity between wetland emissions and anthropogenic emissions is their lack of seasonality (Fig. 22 and Fig. 20). Both emission sources peak during summer months from May to the end of June, and reach a minimum at the end of the year during November-December. The trends from the two individual source emissions are different from the seasonality of total emissions (anthropogenic + wetlands).

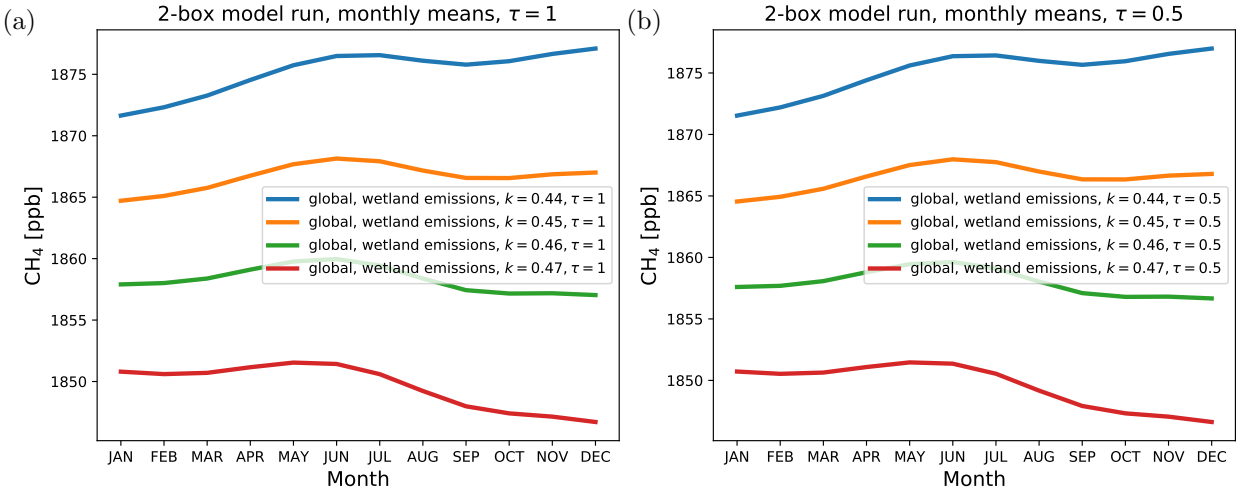

Figure 23: Monthly means of two-box model run of global wetland emissions for 5 years (2010 - 2014) using LCH4 for global values where k and τ are varied.

4 Conclusions

As aformentioned, we quickly discovered that our hypothesis of wetlands acting as the main driver for CH_4 seasonality to be counterfeited simply due to the fact that the peaks and troughs in its trend were inverse (Fig. 5) to methane's observed trend (Fig. 2).

We have shown with our one-box model and use of the total loss variable (LCH4) from GFDL model, that there exists a coherent seasonal cycle of methane when wetland and anthropogenic sources are considered together. We have also shown that we do not observe seasonality in the anthropogenic-only run with any value of k, and that we indeed notice seasonality in the wetland-emissions-only run for all values of k. From our robust findings, we believe wetland emissions play a significant role in the CH_4 seasonality (intra-annual variability).

Running the two-box model with wetland emissions shows similar seasonality as the anthropogenic only run. The two-box model doesn't help us because we have to tune the sink excessively in order to maintain the budget (try to maintain steady state), because as of right now, the RK45 solver time-step is not predetermined in regards to its lack of even time-steps (e.g. if we solve the equation from time-step 0 to 60 months, the solver may use time 0.01 or 0.07). Overall, with the two-box model we see no relationship between the CH_4 seasonality and the model runs under the individual source emissions conditions. One possible scenario is that we need to tune the k parameter to relatively high values ($6.8 < k < 7.1$) and, therefore, amplify the loss by 7-fold to budget the emissions and sinks. However, k was in range $0.98 < k < 1.02$ for the 1-box model and it produced seasonality when we run it with total emissions and wetlands emissions only. Therefore, we believe the one-box model seems to be a better representation of the emissions and sink process; and we can say that it models a more realistic picture of seasonality than the two-box model.

We show that when we use wetlands in the model we have similar seasonality to the observed methane trends, but this can be some sort of correlation related to the sink and we cannot confirm nor deny our hypothesis solely based on this. Though we cannot confirm our idea that wetland emissions drive CH_4 seasonality, we postulate that it can serve as a proxy for CH_4 trending, by reasoning that the system driving wetland emission variability is the same system driving methane seasonality. It is evident that wetlands emissions are correlated with the seasonal CH_4 concentration in the atmosphere, but we currently do not have sufficiently compelling arguments to establish a causality in our study.

5 Additional Notes

It serves to note that wetlands are the largest source of uncertainty regarding the methane budget (Kirschke et al., 2013 and Saunois et al., 2019); with a minimum-maximum range of $107 \frac{Tg\ CH_4}{yr}$ from bottom-up approach for natural wetland emissions (Kirschke et al., 2013). Under the Global Carbon Project, Saunois et al., 2019, asserted a list of priorities to improve the methane budget by minimizing the uncertainties. The relevant three priorities regarding wetland uncertainties are as follows:

1. we need a global, high-resolution map of water-saturated soils and inundated areas emitting methane based on a robust classification of different types of emitting habitats;

2. further development of process-based models for inland-water emissions;

3. intensification of methane observations at local scales (e.g., FLUXNET-CH4 measurements and urban monitoring to constrain bottom-up land surface models, and at regional scales (surface networks and satellites) to constrain atmospheric inversions (Saunois et al., 2019).

Other works have endeavored to address this issue in regards to CH_4 growth, and have shown that global wetland emissions have not significantly contributed to the renewed CH_4 growth despite its uncertainties (Poulter et al., 2017). Poulter et al., 2017, further concurs with similar findings that indicate that a combination of fossil fuel and agriculture sources (Schaefer et al., 2016), as well as a decrease in OH sink, were the reason for the renewed methane growth (Kirschke et al., 2013). We have shown with our simple one- and two-box models, that a combination of anthropogenic (includes agriculture sector) and wetland emissions could be argued to force methane emissions to the observed trends we have seen since 1983. Our findings are similar to the conclusions Kirschke et al., 2013, that asserts, with their use of a more complicated chemistry

model, a rise in natural wetland and fossil fuel emissions were the probable causes for the renewed growth of global methane concentrations from 2007 to present. They note, as we take the opportunity to do the same, that the relative contribution of these two sources continues to elude us (Kirschke et al., 2013).

6 GitHub

All code, data, and this report are is available on GitHub at `https://github.com/imitevski/ch4_box_model`.

7 References

1. P. Bousquet, B. Ringeval, I. Pison, E. J. Dlugokencky, E.-G. Brunke, C. Carouge1, F. Chevallier, A. Fortems-Cheiney, C. Frankenberg, D. A. Hauglustaine, P. B. Krummel, R. L. Langenfelds, M. Ramonet, M. Schmidt, L. P. Steele, S. Szopa1, C. Yver, N. Viovy, and P. Ciais (2011), Source attribution of the changes in atmospheric methane for 2006-2008, Atm. Chem. Phys., 11, `doi.org/10.5194/acp-11-3689-2011`

2. Bousquet, P., Ciais, P., Miller, J. B., Dlugokencky, E. J., Hauglustaine, D. A., Prigent, C., Van der Werf, G. R., Peylin, P., Brunke, E. G., Carouge, C., Langenfelds, R. L., Lathiere, J., Papa, F., Ramonet, M., Schmidt, M., Steele, L. P., Tyler, S. C., and White, J. (2006), Contribution of anthropogenic and natural sources to atmospheric methane variability, Nature 443, `doi:10.1038/nature05132`.

3. Denman, K. L., Brasseur, G., Chidthaisong, A., Ciais, P., Cox, P.M., Dickinson, R. E., Hauglustaine, D., Heinze, C., Holland, E.,Jacob, D., Lohmann, U., Ramachandran, S., da Silva Dias, P. L., Wofsy, S. C., and Zhang, X.: Couplings Between Changes in the Climate System and Biogeochemistry, in: Climate Change 2007: The Physical Science Basis. Contribution of Working Group I to the Fourth Assessment Report of the Intergovernmental Panel on Climate Change, edited by: Solomon, S., Qin, D., Manning, M., Chen, Z., Marquis, M., Averyt, K. B., Tignor, M., and Miller, H. L., Cambridge University Press, Cambridge, UK and New York, NY, USA, 2007. `https://www.ipcc.ch/site/assets/uploads/2018/02/ar4-wg1-chapter7-1.pdf`

4. He, J., V. Naik, L.W. Horowitz, E. Dlugokencky, and K. Thoning (2019), Investigation of the global methane budget over 1980-2017 using GFDL-AM4.1, Atm. Chem. Phys., (preprint), `https://doi.org/10.5194/acp-2019-529`.

5. Kirschke, S., P. Bousquet, P. Ciais, M Saunois, J.G. Canadell, E.J. Dlugokencky, P. Bergamaschi, D. Bergmann, D.R. Blake, L. Bruhwiler, P. Cameron-Smith, S. Castaldi, F. Chevallier, L. Feng, A. Fraser, M. Heimann, E.L. Hodson, S. Houweling, B. Josse, P.J. Fraser, P.B. Krummel, J. Lamarque, R.L. Langenfelds, C. Le Quéré, V. Naik, S. O'Doherty, P.I. Palmer, I. Pison, D. Plummer, B. Poulter, R.G. Prinn, M. Rigby, B. Ringeval, M. Santini, M. Schmidt, D.T. Shindell, I.J. Simpson, R. Spahni, L.P. Steele, S.A. Strode, K. Sudo, S. Szopa, G.R. van der Werf, A. Voulgarakis, M. van Weele, R.F. Weiss, J.E. Williams, and G. Zeng (2013), Three decades of global methane sources and sinks, Nature Geosci, 6, `doi.org/10.1038/ngeo1955`.

6. National Oceanic and Atmospheric Administration, Global CH_4 monthly means (2019), NOAA figure.

7. Nisbet, E.G., E.J. Dlugokencky, M.R. Manning, D. Lowry, R.E. Fisher, J.L. France, S.E. Michel, J.B. Miller, J.W.C. White, B. Vaughn, P.Bousquet, J.A. Pyle, N.J. Warwick, M. Cain, R. Brownlow, G. Zazzeri, M. Lanoisellé, A.C. Manning, E. Gloor, D.E.J. Worthy, E.-G. Brunke, C. Labuschagne, E.W. Wolff, and A.L. Ganesan (2016), Rising atmospheric methane: 2007–2014 growth and isotopic shift, Global Biochem. Cycles, 30, `doi:10.1002/2016GB005406`.

8. Poulter, B., P. Bousquet, J.G. Canadell, P.Ciais, A. Peregon, M. Saunois, V.K. Arora, D.J. Beerling, V. Brovkin, C.D Jones, F. Joos, N. Gedney, A. Ito, T. Kleinen, C.D. Koven, K. McDonald, J.R. Melton, C. Peng, S.Peng, C. Prigent, R. Schroeder, W.J. Riley, M. Saito, R. Spahni, H. Tian, L.

Taylor, N. Viovy, D. Wilton, A. Wiltshire, X. Xu, B. Zhang, Z. Zhang, and Q. Zhu (2017), Global wetland contribution to 2000–2012 atmospheric methane growth rate dynamics, Environ. Res. Lett., 12, doi.org/10.1088/1748-9326/aa8391.

9. Saunois, M., Stavert, A. R., Poulter, B., Bousquet, P., Canadell, J. G., Jackson, R. B., Raymond, P. A., Dlugokencky, E. J., Houweling, S., Patra, P. K., Ciais, P., Arora, V. K., Bastviken, D., Bergamaschi, P., Blake, D. R., Brailsford, G., Bruhwiler, L., Carlson, K. M., Carrol, M., Castaldi, S., Chandra, N., Crevoisier, C., Crill, P. M., Covey, K., Curry, C. L., Etiope, G., Frankenberg, C., Gedney, N., Hegglin, M. I., Höglund-Isaksson, L., Hugelius, G., Ishizawa, M., Ito, A., Janssens-Maenhout, G., Jensen, K. M., Joos, F., Kleinen, T., Krummel, P. B., Langenfelds, R. L., Laruelle, G. G., Liu, L., Machida, T., Maksyutov, S., McDonald, K. C., McNorton, J., Miller, P. A., Melton, J. R., Morino, I., Müller, J., Murgia-Flores, F., Naik, V., Niwa, Y., Noce, S., O'Doherty, S., Parker, R. J., Peng, C., Peng, S., Peters, G. P., Prigent, C., Prinn, R., Ramonet, M., Regnier, P., Riley, W. J., Rosentreter, J. A., Segers, A., Simpson, I. J., Shi, H., Smith, S. J., Steele, L. P., Thornton, B. F., Tian, H., Tohjima, Y., Tubiello, F. N., Tsuruta, A., Viovy, N., Voulgarakis, A., Weber, T. S., van Weele, M., van der Werf, G. R., Weiss, R. F., Worthy, D., Wunch, D., Yin, Y., Yoshida, Y., Zhang, W., Zhang, Z., Zhao, Y., Zheng, B., Zhu, Q., Zhu, Q., and Zhuang, Q.: The Global Methane Budget 2000–2017, Earth Syst. Sci. Data Discuss., doi.org/10.5194/essd-2019-128, in review, 2019.

10. Saunois, M., R.B. Jackson, P. Bousquet, and J.G. Canadell (2016), The growing role of methane in anthropogenic climate change, Environ. Res. Lett., 11, http://dx.doi.org/10.1088/1748-9326/11/12/120207.

11. Schaefer1, H, S.E. Mikaloff Fletcher, C. Veidt, K.R. Lassey, G.W. Brailsford, T.M. Bromley, E.J. Dlugokencky, S.E. Michel, J.B. Miller, I. Levin, D.C. Lowe, R.J. Martin, B.H. Vaughn, J.W.C. White (2016), 21st century shift from fossil-fuel to biogenic methane emissions indicated by $13CH_4$, Science, 352, 10.1126/science.aad2705.